PERGAMON

International Journal of Heat and Mass Transfer 42 (1999) 1835–1847

International Journal of HEAT and MASS TRANSFER

Critical heat flux in a long, rectangular channel subjected to one-sided heating—I. flow visualization

J. Christopher Sturgis, Issam Mudawar*

Boiling and Two-Phase Flow Laboratory, School of Mechanical Engineering, Purdue University, West Lafayette, IN 47907, U.S.A.

Received 12 February 1998; in final form 3 August 1998

Abstract

Flow boiling in a straight, rectangular channel was investigated to explore the conditions leading to critical heat flux (CHF). The flow channel had a 5.0×2.5 mm cross-section and 101.6 mm heated length; heat was applied to the shorter dimension along only one wall. Tests were performed with FC-72 liquid over a velocity range of 0.25 to 10 m s^{-1} and at outlet subcoolings of 3, 16 and 29°C. Video images captured at CHF at various flow conditions revealed that vapor coalesces into a series of patches resembling a wavy vapor layer which propagates along the heated wall allowing liquid to contact the wall only at discrete locations. Measurements indicate that vapor patch length, vapor patch height and liquid contact length increase along the flow direction but decrease with increasing subcooling and velocity. The measurements also reveal that the ratio of liquid-to-vapor length remains approximately constant along the heated wall for a particular subcooling. These observations and measurements represent key contributions to critical heat flux modeling efforts presented in Part II of this study.

Nomenclature

C_1, C_2 constants in eqn. (1)
b ratio of liquid-to-vapor length of wavy liquid–vapor interface
d_{up} measured distance from heater inlet to upstream edge of vapor patch
D_h hydraulic diameter of channel
L length of heater
l length of liquid–surface contact (wetting front) for CHF modeling
l_{meas} measured liquid length between vapor patches
P_o fluid pressure at outlet of heated section
q'' heat flux
q''_m maximum nucleate boiling heat flux, CHF
Re_D Reynolds number, $[U D_h/\nu_f]$
T temperature
T_b fluid bulk temperature
T_o fluid temperature at outlet of heated section
$T_{sat,o}$ fluid saturation temperature (at P_o) at outlet of heated section
T_w wall temperature
$\Delta T_{sub,i}$ fluid subcooling at inlet of heated section
$\Delta T_{sub,o}$ fluid subcooling at outlet of heated section at CHF
U average inlet liquid velocity
x coordinate perpendicular to fluid–surface interface.

Greek symbols
δ vapor layer amplitude for CHF modeling
δ_{meas} measured vapor patch height
λ vapor wavelength for CHF modeling
λ_{meas} measured vapor patch length
ν_f kinematic viscosity of liquid.

1. Introduction

Maintaining heat loads below the critical heat flux is crucial for the reliable operation of many thermal devices. Therefore, the prediction of this thermal limit provides necessary information for the design and operational phases of such devices. These predictions are often based on correlations developed from experimental data and, as such, may be limited by the physical conditions and parametric ranges under which the correlations were

* Corresponding author. Tel.: 001 765 494 5705; fax: 001 765 494 0539; e-mail: mudawar@ecn.purdue.edu

0017–9310/98/$ - see front matter
PII: S0017–9310(98)00274–9

developed. It is therefore desirable to develop a mechanistic model which incorporates fundamental parameters to predict the critical heat flux limit. It is the specific purpose of the present two-part study to model flow boiling CHF in a long, rectangular channel, drawing on results of the extensive flow visualization study presented here.

In their development of the interfacial lift-off model, Galloway and Mudawar [1, 2] utilized flow visualization techniques to describe vapor behavior at CHF. They used a high speed camera to capture the boiling of FC-87 on a short heater ($L = 12.7$ mm) for low velocity and near-saturated conditions. The camera captured a side view of the channel permitting the observation of a wavy vapor layer and the measurements of vapor height and length.

Gersey and Mudawar [3, 4] extended the flow visualization work of Galloway and Mudawar to long, straight heaters ($L = 10$, 30 and 110 mm) also observing a periodic nature to the vapor distribution. In their study, the view was normal to the heated wall which precluded measuring vapor height. Their tests concentrated on low velocity ($U \leqslant 2$ m s^{-1}) and neat-saturated conditions ($\Delta T_{\mathrm{sub,i}} = 4^{\circ}$C).

The present flow visualization study complements these earlier ones by extending flow visualization to higher velocities ($U = 0.24$–4.0 m s^{-1}), subcooled conditions ($\Delta T_{\mathrm{sub,o}} = 3$ and 29°C) and long heaters ($L = 101.6$ mm). Video images were obtained from a side view permitting the observation and measurement of vapor along the entire heated length. With the significant amount of images obtained, dominant features were realized through visual and statistical means. This paper is the first of a two-part study describing an extended version of the interfacial lift-off model first proposed by Galloway and Mudawar [2]. Part II of this study [5] details the development of a CHF model incorporating the flow visualization results.

2. Experimental methods

2.1. Experimental apparatus

The heated portion of the straight, rectangular channel used for testing is shown in Fig. 1. The flow channel was formed by bolting together two plates of opaque, high-temperature G-10 fiberglass plastic, only the bottom plate is shown in Fig. 1. Into the bottom plate was machined a long groove having a 5.0×2.5 mm rectangular cross-section. A portion of one side wall of the groove was removed so that a copper heater could be inserted. With the aid of a microscope, the straight wall of the heater was carefully aligned flush with the interrupted wall of the groove to form a continuous, rectangular flow channel. A flexible Teflon cord placed in a shallow O-ring groove on the underside of the top plate sealed the channel when the two plates were bolted together. When fully assembled, the flow channel had a 101.6 mm long heated wall preceded by an adiabatic, hydrodynamic entry length measuring 106 hydraulic diameters. Flow instrumentation consisted of thermocouples and pressure transducers, connected via fittings attached to the top plate, to measure conditions just upstream and downstream of the heated length.

The heater was made from a single piece of 99.99% pure oxygen-free copper. Power was supplied by cylindrical cartridge heaters embedded in the heater's thick portion as shown in Fig. 1. The four cartridge heaters were connected to a 240 volt variac allowing power to be incremented during testing. Distributing the cartridge heaters symmetrically and using copper for the heater block ensured power was evenly distributed along the heated surface, which measured 2.5 mm in width and 101.6 mm along the flow direction.

The integral channel/heater assembly was tested in the closed, two-phase flow loop shown schematically in Fig. 2. A centrifugal pump circulated FC-72 liquid from the large reservoir through the main and test section subloops which contained the indicated filters, heat exchangers, control valves, flow meters and flow channel. System pressure could be adjusted by forcing FC-72 vapor, generated in a pressurized tank, into the reservoir. In this manner, no gas other than FC-72 vapor was needed in the pressurization, thereby maintaining a pure working fluid. The use of FC-72 liquid, a dielectric Fluorinert manufactured by the 3M Company, was based upon its low boiling point (57°C at 1 atm) and relatively low heat of vaporization requiring only a modest heat input to achieve boiling.

2.2. Data reduction

In order to determine local wall flux and wall temperature, three Type-K thermocouples were inserted at each of five locations along the heater as illustrated in Fig. 1. At each location, the thermocouple beads were epoxied into small holes which were precisely drilled with respect to each other and the heated wall. Assuming one-dimensional conduction through the thin portion of the copper heater, a temperature profile was calculated based on these three measurements. A least-squares best-fit analysis was used to determine the linear profile given by

$$T(x) = C_1 x + C_2, \tag{1}$$

where $x = 0$ indicates the heated surface. With the profile established, the calculations of wall heat flux, q'', and wall temperature, T_{w}, at a given location were straightforward, with a constant copper conductivity of 391 W m^{-1} K^{-1} assumed.

The inlet fluid temperature, T_{in}, was measured by the

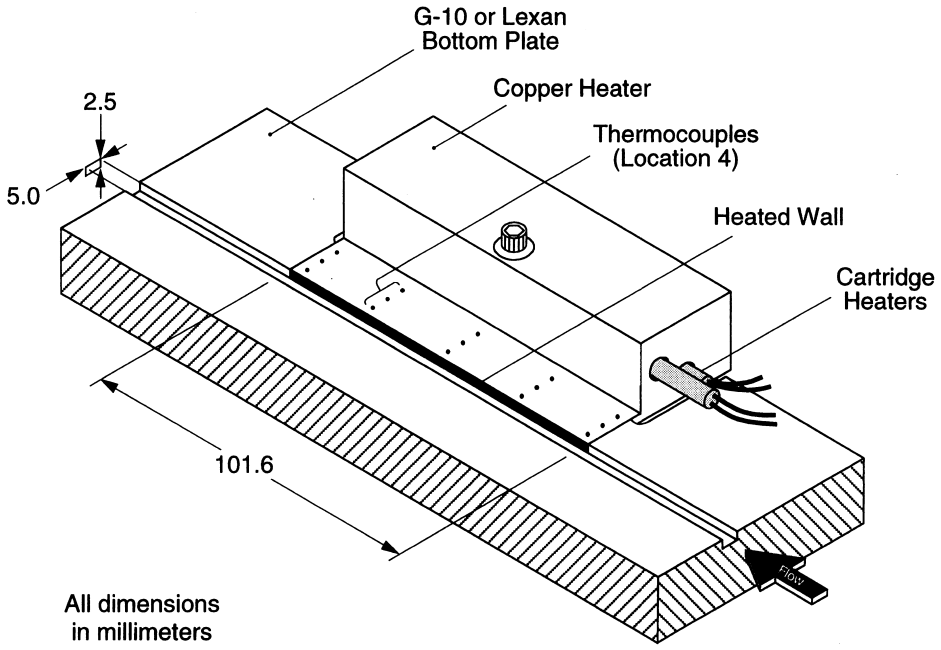

Fig. 1. Heated section of rectangular flow channel.

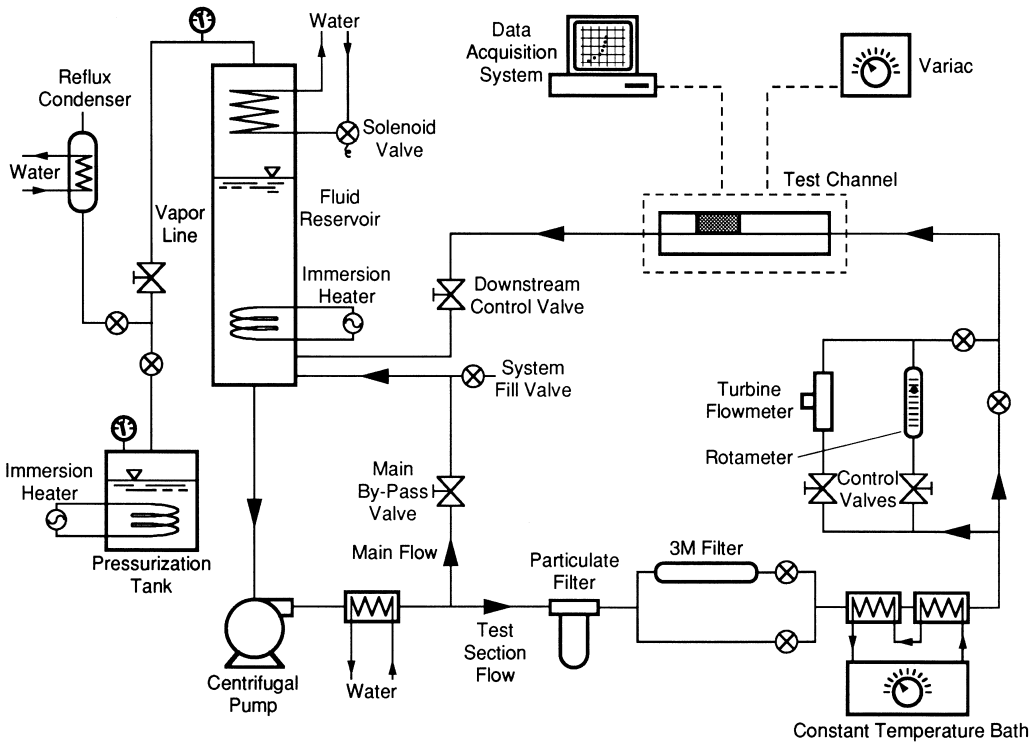

Fig. 2. Closed, two-phase flow loop and auxiliary components.

upstream thermocouple. In lieu of inserting thermocouples along the channel to measure flow temperatures, the bulk fluid temperature, T_b, at each location and the outlet temperature, T_o, were calculated assuming thermodynamic equilibrium.

The critical heat flux, q''_m, was defined as the largest steady-state flux attained during testing. At CHF, vapor covered the surface essentially insulating it. Consequently, heat supplied by the cartridge heaters could not be removed by the liquid and remained in the copper to cause a temperature rise and gradient decrease. Hence, CHF was detected during testing by an unsteady increase in calculated wall temperature accompanied by a sudden decrease in calculated wall flux.

2.3. Test conditions

The fluid in the loop was deaerated to remove non-condensable gases prior to each series of tests. After adjusting inlet temperature, outlet pressure and flow rate to desired values, the applied power was incremented beginning at a low setting. A data point was recorded at each power setting once hydrodynamic and thermal conditions were deemed steady. Testing progressed through the single- and two-phase heat transfer regimes (generating a boiling curve) and was terminated immediately after the detection of critical heat flux.

Critical heat fluxes were obtained for a test matrix consisting of three outlet subcoolings ($\Delta T_{sub,o} = 3$, 16 and 29°C) and 13 flow velocities ($U = 0.25$ to 10 m s^{-1}). $\Delta T_{sub,o}$ refers to the prevailing subcooling value at the outlet of the heated section at the time of critical heat flux. For all tests, the outlet pressure was held constant at $P_o = 1.38$ bar, resulting in a constant FC-72 saturation temperature of $T_{sat,o} = 66.3$°C. The inlet temperature remained constant during a particular test and was chosen such that the outlet temperature equaled its desired value at CHF.

Reynolds number based on hydraulic diameter and inlet conditions, $Re_D = UD_h/v_f$, ranged from 2,000 to 130,000. Considering these values and the fact that the hydrodynamic entry length measured over 100 hydraulic diameters, fully-developed turbulent flow was assumed to exist at the heater inlet. For the range of velocity tested, the corresponding mass flux ranged from 400 to 16,800 kg m^{-2} s^{-1} and fluid inlet temperature varied from 48 to 62, 32 to 49 and 17 to 35°C corresponding to outlet subcoolings of 3, 16 and 29°C, respectively.

The channel was tested in a horizontal position with the gravity vector oriented parallel to the heated surface and perpendicular to bulk motion. Movement of vapor due to gravity-induced buoyancy forces was restricted due to the narrow channel width. Therefore, effects of gravity on vapor motion, formation and coalescence were considered negligible compared to surface tension, frictional and inertial forces.

2.4. Repeatability and uncertainty analysis

The procedures for assembling the channel and acquiring data were consistent throughout the test program. Boiling curves for duplicated tests were nearly identical indicating repeatable results, negligible aging of the heater and consistent assembly procedures. Multiple CHF values obtained for particular conditions were always within 3.4% of their averages. This is less than the calculated uncertainty in heat flux, which was approximately 8.5% at low fluxes ($q'' \approx 30$ W cm^{-2}) and decreased to less than 5% at high fluxes ($q'' \approx 150$ W cm^{-2}). Wall temperature calculations were accurate to within 0.3°C and flowrate uncertainty was less than 2.3%. The assumption of one-dimensional conduction through the copper heater proved reasonable since the difference in calculated fluxes among the five locations was in most cases less than the uncertainty.

Heat losses from the large, exposed faces of the copper heater were not of concern since heat flux was not derived from electrical power input but rather the temperature profile based on thermocouple readings. Numerical modeling revealed the losses from the thin, instrumented segment represented only about 5% of the heat flowing into this segment for low fluxes ($q'' \approx 15$ W cm^{-2}) and even less for high fluxes.

3. Critical heat flux data

The boiling curves in Fig. 3 display the two-phase characteristics of the rectangular flow channel with respect to velocity. The incipient boiling heat flux and critical heat flux, q''_m, both increased with increasing

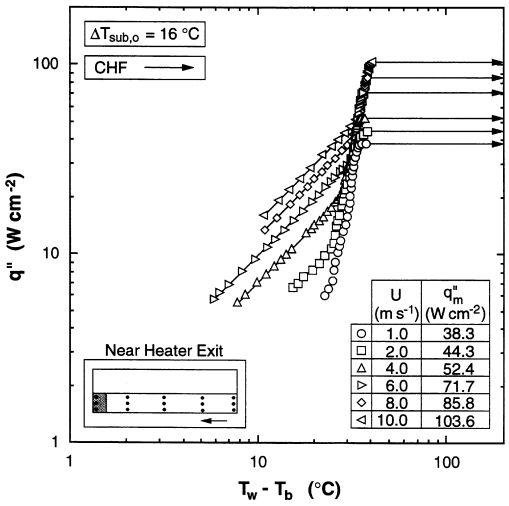

Fig. 3. Boiling curves near heater exit for $\Delta T_{sub,o} = 16$°C and select velocities.

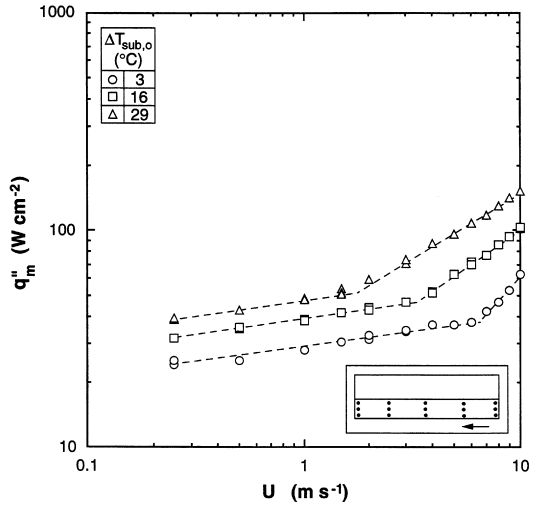

Fig. 4. Critical heat flux data for rectangular flow channel.

velocity. Increasing fluid subcooling also increases the incipience boiling flux and CHF while shifting the nucleate boiling regime to higher wall temperature differences. These effects are due to the cooler bulk fluid postponing vapor production and more readily condensing vapor bubbles.

Critical heat fluxes for all tests are presented in Fig. 4 which shows the effects of velocity and outlet subcooling. CHF increased with increasing velocity showing two distinct slopes for each subcooling. As shown by the dashed lines, the relationship in each regime is linear (on a log-lot plot) with the change in slope being delayed to higher velocities as the subcooling is lowered. Maddox and Mudawar [6] noted the same change in scope for data obtained with a short heater. Though not confirmed directly by flow visualization at high velocities, the change in slope of the present CHF data is most likely related to the thinning of the vapor layer. The data showed CHF increasing linearly with outlet subcooling, a conclusion supported by the work of Wu and Simon [7] and Collier and Thorne [8].

4. Flow visualization analysis

4.1. Flow visualization equipment and procedure

In order to gain insight into the relationship between vapor dynamics and critical heat flux, a visual investigation of the flow boiling process was initiated. A second channel was fabricated from optical-grade polycarbonate (brand name Lexan MP750) with the same design as that used to obtain the CHF data. Tests with this clear channel used the same heater, instrumentation, fluid and flow loop, the only difference being optical access to the heated length.

A Canon L1 8 mm video camera was used to capture the flow boiling process. Its lens was positioned a few millimeters above the channel by attaching the base of the camera to a cantilevered beam that was secured to a Questar tripod, as illustrated in Fig. 5. The tripod was equipped with translation stages allowing the camera to be moved in the three coordinate directions, thus enabling the entire heated length to be traversed. Video sequences were recorded with a 30× lens at a rate of 30 frames per second and a shutter speed of 1/10,000 of a second. The high shutter speed essentially froze the flow capturing crisp images with the aid of a high intensity light source. The view through the camera was parallel to the heated surface and perpendicular to the flow direction. Approximately 30 mm of the channel length were captured in a frame, so the 101.6 mm heated length was videotaped in four segments by traversing the camera. This magnification served as a good compromise for analyzing the frames. A higher magnification would have made it difficult to observe vapor development and long vapor patches whereas a lower magnification would have compromised the accuracy of the vapor measurements.

For each flow visualization test, the heated length was videotaped in four segments with the bubble characteristics at CHF analyzed and categorized. Due to the relatively slow frame rate, motion sequencing was not possible except at the lowest test velocity. This precluded observing frame-by-frame a particular vapor patch/

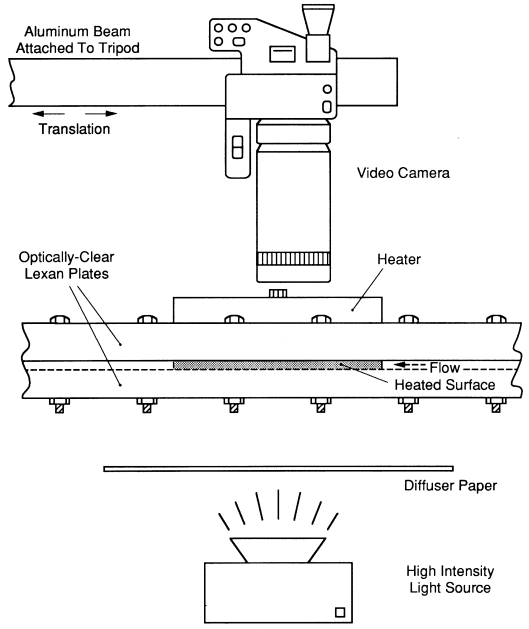

Fig. 5. Camera and channel arrangement for flow visualization tests.

bubble as it moved through the channel. Nevertheless, video allowed for the collection of significantly more frames of vapor activity than could be obtained with still photography. This proved to be a tremendous asset in conducting the statistical analysis of vapor size, shape and percentage of occurrence.

Video sequences were obtained for only the near-saturated ($\Delta T_{sub,o} = 3°C$) and highly subcooled ($\Delta T_{sub,o} = 29°C$) cases for velocities of $U = 0.25$, 1, 2 and 4 m s^{-1}. Higher velocities were not attempted since vapor dimensions were approaching sizes too small to be measured reliably and since the integrity of the polycarbonate channel would be compromised at the higher wall temperatures associated with higher velocities. Small holes precisely drilled near the edge of the channel and captured in the video provided a scale by which to make measurements of bubble dimensions. These measurements were obtained manually using a video monitor and a ruler constructed for each test based on the known spacing of the small holes.

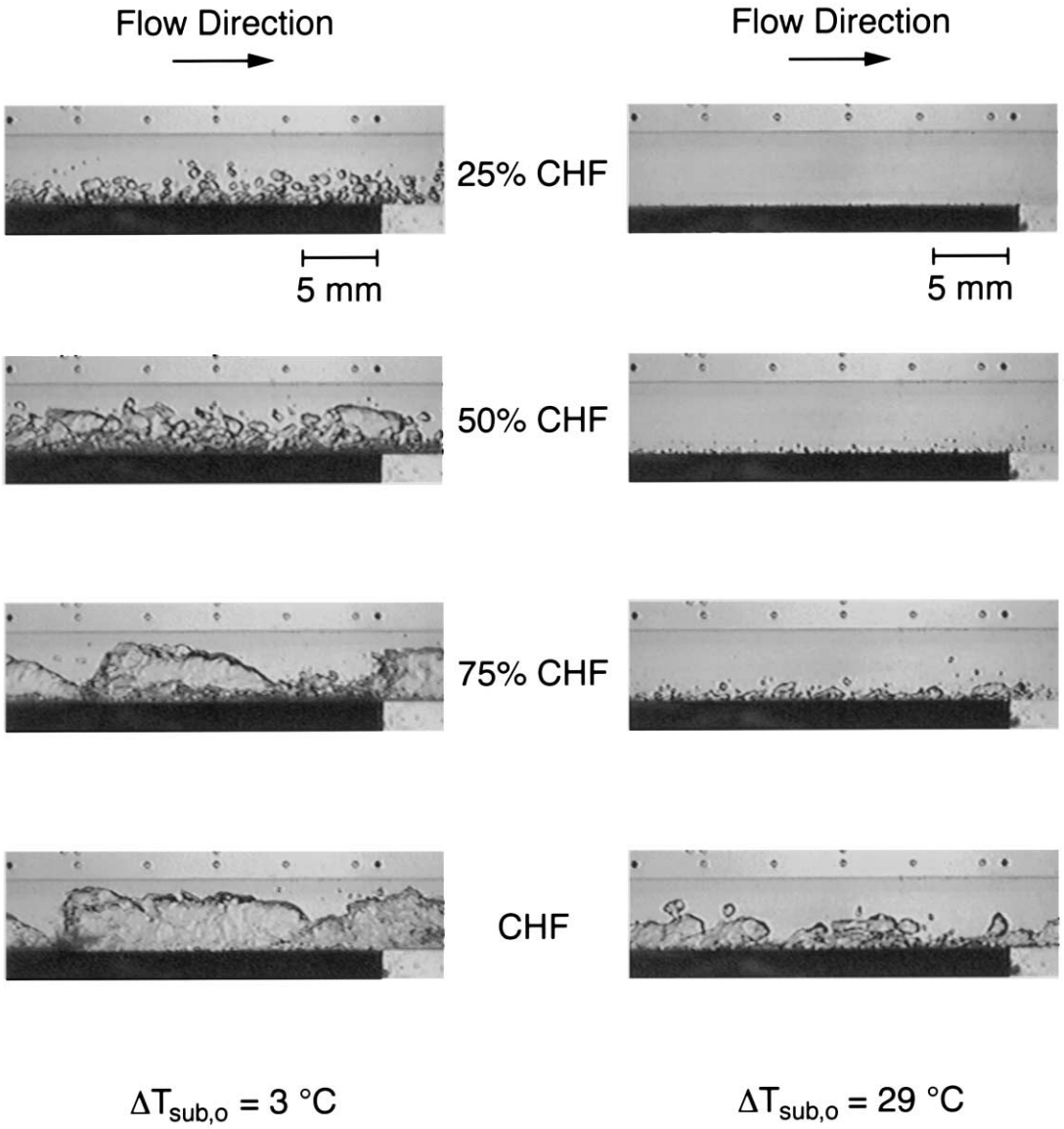

Fig. 6. Video images of flow boiling at downstream segment of heater at different heat fluxes for $U = 1$ m s^{-1} for near saturated ($\Delta T_{sub,o} = 3°C$) and subcooled ($\Delta T_{sub,o} = 29°C$) conditions.

4.2. Flow boiling images

Vapor development along the heated length was examined with respect to streamwise location, heat flux, flow velocity and subcooling. The figures discussed in this section, Figs 6–8, are video images representing typical observations of vapor in the channel for the conditions indicated. Channel height is 5.0 mm and width (depth of view into page) is 2.5 mm. The dark region along the channel is the heater with upstream and downstream adiabatic sections of channel shown with a lighter shade. The small holes used for constructing a measurement scale are visible along the edge of the channel.

The behavior of vapor near the exit of the heated length with increasing flux is shown in Fig. 6 for $\Delta T_{\mathrm{sub,o}} = 3$ and 29°C at $U = 1$ m s^{-1}. For the neat-saturated case at 25% of CHF, vapor mainly took the form of small, discrete bubbles which did not represent a significant impediment to the rewetting liquid. But as the flux increased, the bubbles coalesced and formed larger masses, eventually covering large lengths of the surface at 75% of CHF. At critical heat flux, these patches grew into a periodic, wave-like vapor layer which prevented the liquid from reaching the surface except over short lengths refered to as wetting fronts. A similar behavior is shown in Fig. 6 for $\Delta T_{\mathrm{sub,o}} = 29$°C except that the vapor height is smaller due to the cooler bulk limiting vapor production and condensing vapor previously generated.

Figure 7 shows flow boiling in the channel at CHF for near-saturated ($\Delta T_{\mathrm{sub,o}} = 3$°C) and subcooled ($\Delta T_{\mathrm{sub,o}} = 29$°C) conditions at a bulk velocity of $U = 1$ m s^{-1}. Flow is from left to right and the channel is flush with the heater at the inlet though the edge is not visible. As clearly shown, vapor coalesced into patches which grew in size along the heated wall as a result of continual vapor production. The vapor remained in contact with the surface restricting liquid access to the heater, especially for the near-saturated case. Vapor length and height are observed to decrease with increasing subcooling. The series of vapor patches display an undulating, periodic nature which is the basis of the idealized wavy interface adopted in the modeling effort described in part II of this study [5].

Figure 8 shows the changes in vapor characteristics with increasing velocity for near-saturated and subcooled conditions. These images are of the downstream segment of the heater at the critical heat flux corresponding to each condition indicated. The decrease in vapor length with increasing velocity is clearly noticeable. Likewise, the vapor height decreased even though CHF increased with increasing velocity. No vapor measurements were possible for $U \geqslant 4$ m s^{-1} at $\Delta T_{\mathrm{sub,o}} = 29$°C.

4.3. Vapor measurements

Vapor patches were measured from 50 frames for each heater segment at various flow conditions in an effort to quantify the observations discussed above. Particular characteristics of interest were vapor length, λ_{meas}, maximum height, δ_{meas}, and location of upstream edge, d_{up}, as well as length of liquid-surface contact between adjacent patches, l_{meas}, as illustrated in Fig. 9. In some cases, the identification of a vapor patch itself was difficult since boundaries were not always distinct. However, the collection of numerous measurements allowed for a

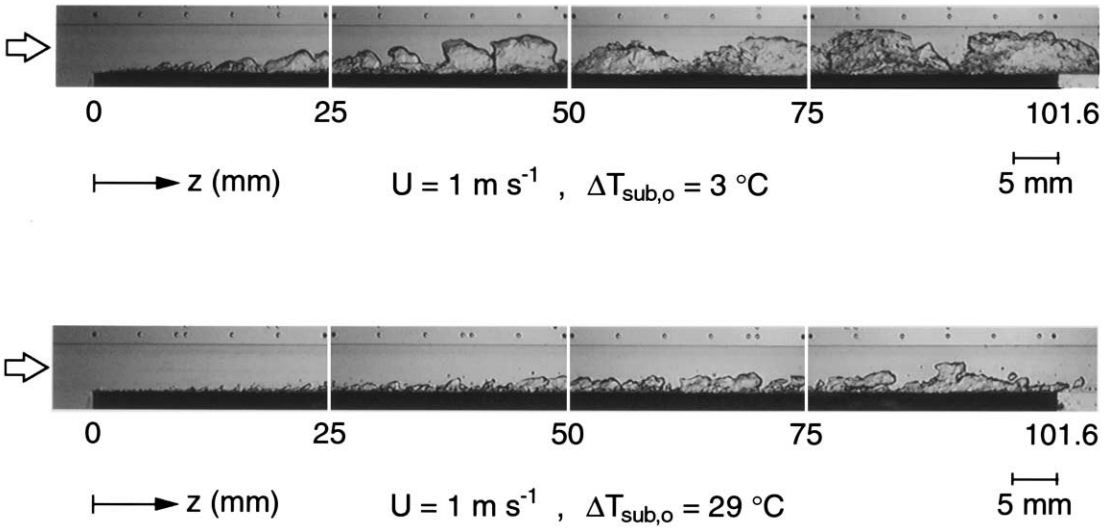

Fig. 7. Video images of flow boiling at CHF at $U = 1$ m s^{-1} for near saturated ($\Delta T_{\mathrm{sub,o}} = 3$°C) and subcooled ($\Delta T_{\mathrm{sub,o}} = 29$°C) conditions.

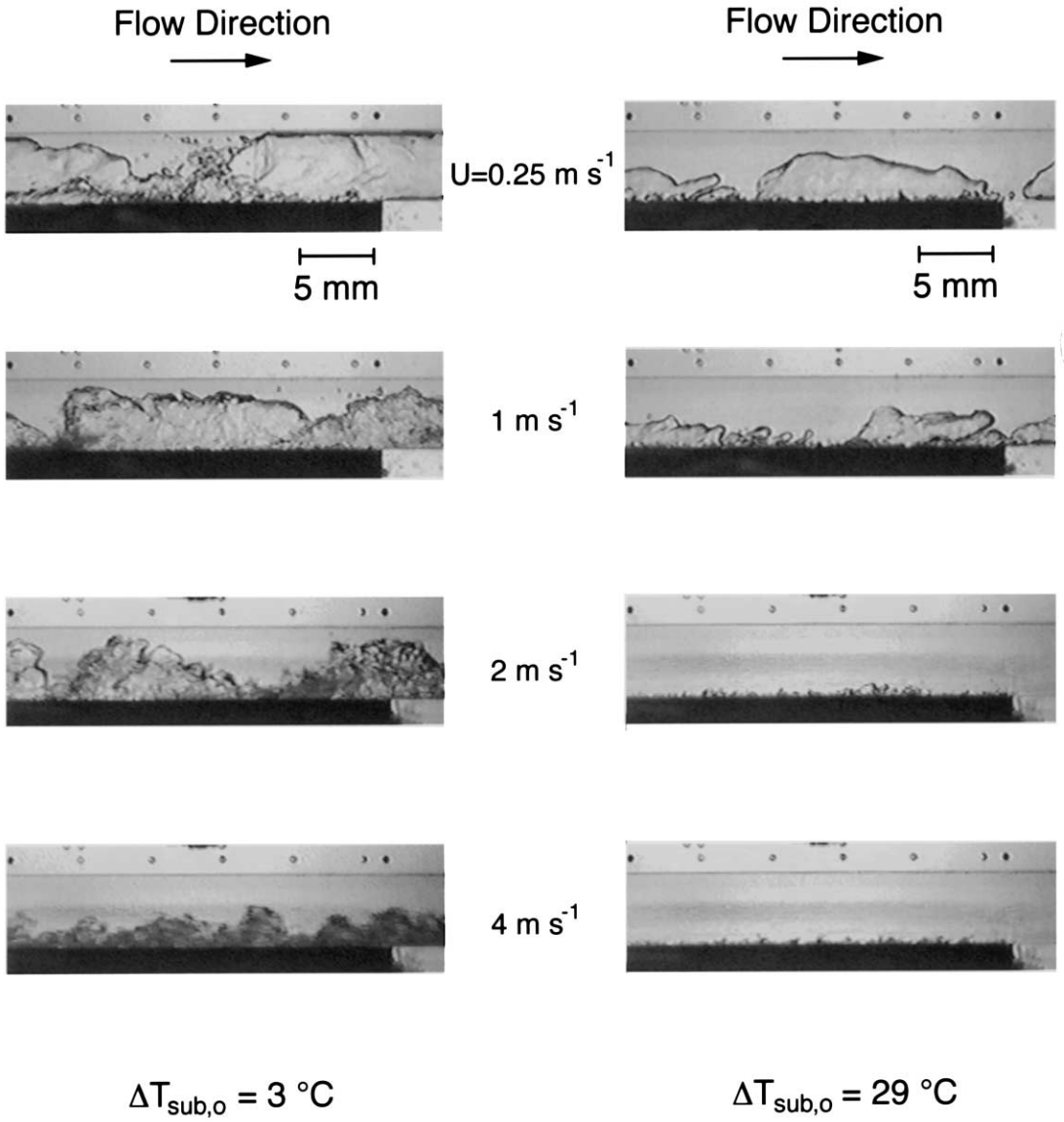

Fig. 8. Video images of flow boiling at downstream segment of heater at CHF for $U = 0.25$, 1, 2 and 4 m s^{-1} for near-saturated ($\Delta T_{\mathrm{sub,o}} = 3$°C) and subcooled ($\Delta T_{\mathrm{sub,o}} = 29$°C) conditions.

statistical analysis of vapor characteristics at CHF that identified characteristics not apparent in a few frames.

Individual measurements for vapor length are plotted in Fig. 10(a) for $\Delta T_{\mathrm{sub,o}} = 3$ and 29°C at $U = 1$ m s^{-1}, with the x-axis representing the location on the heater of the center of the measured patch. Although there is some overlap among the data, two trends are apparent. First, vapor length increased in the flow direction due to vapor generation and coalescence. For each subcooling, the length appears to be reaching an asymptotic value downstream which is consistent with the observations made by Gersey and Mudawar [3] on their 110 mm heater. Secondly, vapor length decreased with increasing subcooling. The cooler bulk reduces vapor production as well as recondenses portions of vapor already present leading to smaller patches on the surface. Figure 10(b) illustrates the effect of velocity on the vapor length for the near-saturated case. The length is consistently shorter for $U = 4$ m s^{-1} due to the increased shear tending to break apart larger vapor masses.

Vapor height increased in the streamwise direction due to the conversion of mass to the vapor phase, as indicated

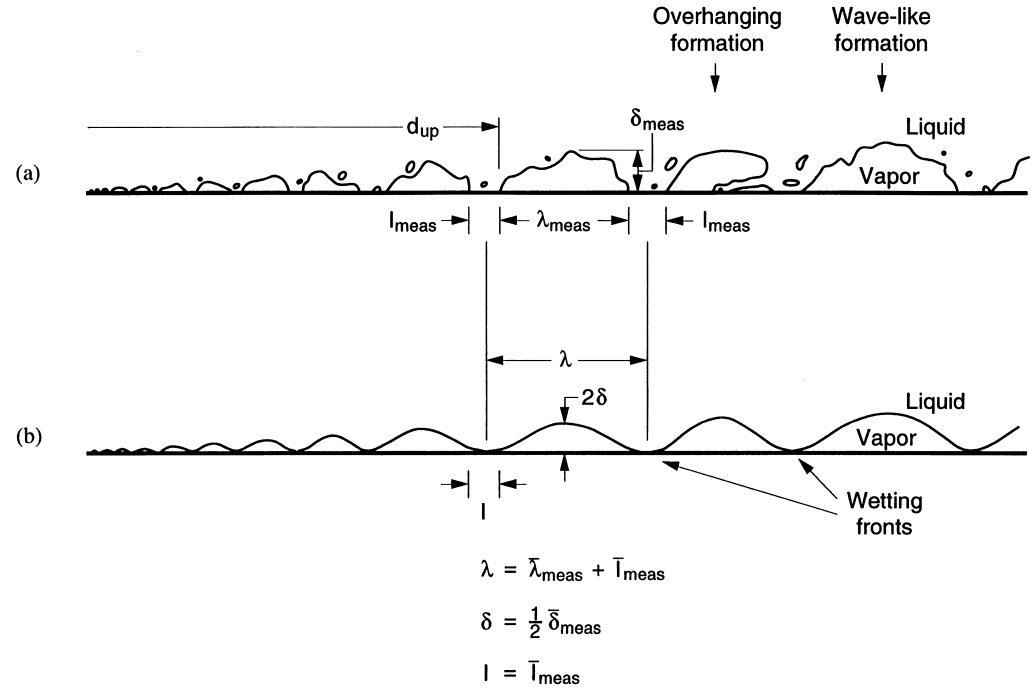

Fig. 9. Definitions of vapor and liquid dimensions as (a) measured in flow visualization study and (b) defined for idealized wavy vapor layer of CHF model presented in part II of this study [5].

by the measurements in Fig. 11(a) for near-saturated ($\Delta T_{sub,o} = 3°C$) and subcooled ($\Delta T_{sub,o} = 29°C$) conditions at $U = 1$ m s^{-1}. For near-saturated flow, the vapor was constrained by the channel dimensions as it grew in thickness to nearly contact the adiabatic wall. As with the vapor length, vapor height was reduced for subcooled flow.

Velocity had a similar effect. Figure 11(b) shows vapor height was reduced and coalescence delayed to farther downstream when velocity was increased from $U = 1$ to 4 m s^{-1} for $\Delta T_{sub,o} = 3°C$. This decrease in vapor height occurred despite a 30% increase in critical heat flux for the higher velocity.

The large collection of measurements obtained in the course of flow visualization testing was analyzed in terms of statistical averages. For each videotaped heater segment with sufficient number of observations (30–200 vapor patches per segment), averages of vapor length, $\bar{\lambda}_{meas}$, vapor height, $\bar{\delta}_{meas}$, and liquid length $\bar{l}_{meas}$, were calculated. Each average value must be viewed carefully since it included all measurements made for a 25 mm segment, over which the vapor length and height were both growing. Nevertheless, these values do provide important information regarding the behavior of the vapor layer along the heater.

The real benefit of these averages is that they provide a key physical contribution to the CHF modeling effort. Obtaining averages for each of the four segments allowed the heated length to be discretized for the construction of an energy balance, an important component of the CHF model [5]. This model uses slightly different definitions for vapor dimensions than those presented in the preceding plots. In anticipation of modeling the series of vapor patches as a wavy interface characterized by a wavelength, λ, and amplitude, δ, the following definitions relate the measured quantities to the idealized interfacial parameters.

$$\lambda = \bar{\lambda}_{meas} + \bar{l}_{meas} \tag{2}$$

$$\delta = \frac{1}{2}\bar{\delta}_{meas} \tag{3}$$

$$l = \bar{l}_{meas} \tag{4}$$

These relationships are shown in Fig. 9. The idealized wavelength is defined as the distance between consecutive wetting fronts, hence it is the sum of average vapor length and average liquid length. When approximating the series of observed vapor patches with a sinusoidal profile, the interfacial amplitude is half the measured height. The wetting region is actually a portion of the idealized wavelength and has the same length as the average measured liquid length.

Statistical averages reveal that the liquid length increased in proportion to the vapor length such that it

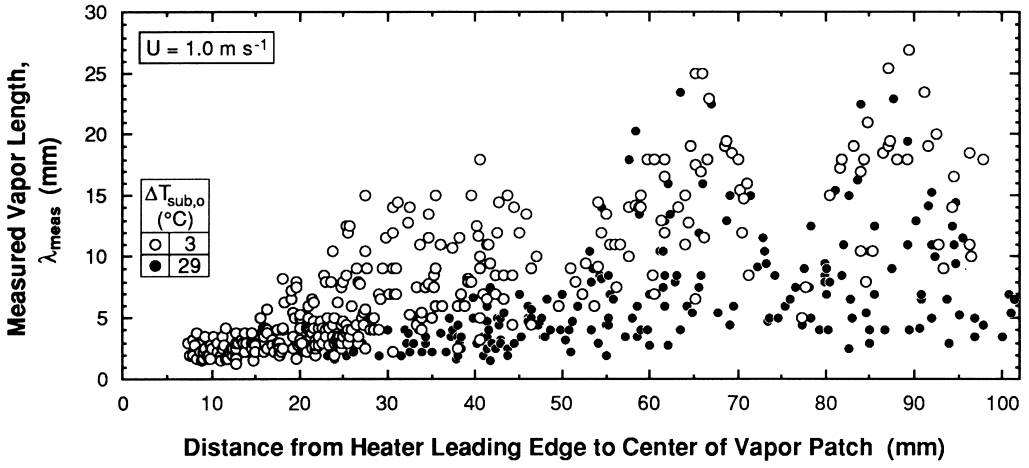

(a)

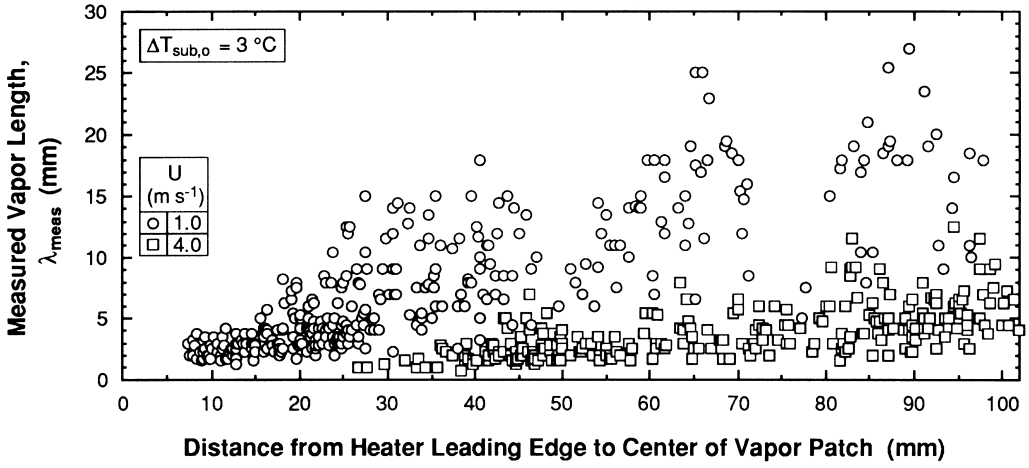

(b)

Fig. 10. Effect of (a) subcooling and (b) velocity on vapor development as indicated by the measured lengths of all vapor patches observed at CHF.

remained approximately the same fraction of the interfacial wavelength, λ. This is indicated by the ratio b, defined as

$$b = \left(\frac{\text{wetting front length}}{\text{vapor wavelength}}\right) = \frac{l}{\lambda}. \quad (5)$$

Furthermore, this ratio showed little sensitivity to velocity, maintaining a value of $b \approx 0.2$ over the entire range of velocity for $\Delta T_{\text{sub,o}} = 3^{\circ}\text{C}$. This implies that a single value for b may be approximated for a particular subcooling, a conclusion supported by data at other subcoolings and velocities. This observation regarding the liquid-to-vapor length ratio has important consequences for the CHF model.

As the velocity increased, vapor production and coalescence were not appreciable until farther downstream, making measurements impossible for certain segments. This occurred at $U = 4$ m s^{-1} for the near-saturated case and as early as $U = 2$ m s^{-1} for the highly subcooled condition. Unfortunately, flow visualization data for the subcooled flow were limited to only a few velocity cases. The limited data do show increasing wavelength, height

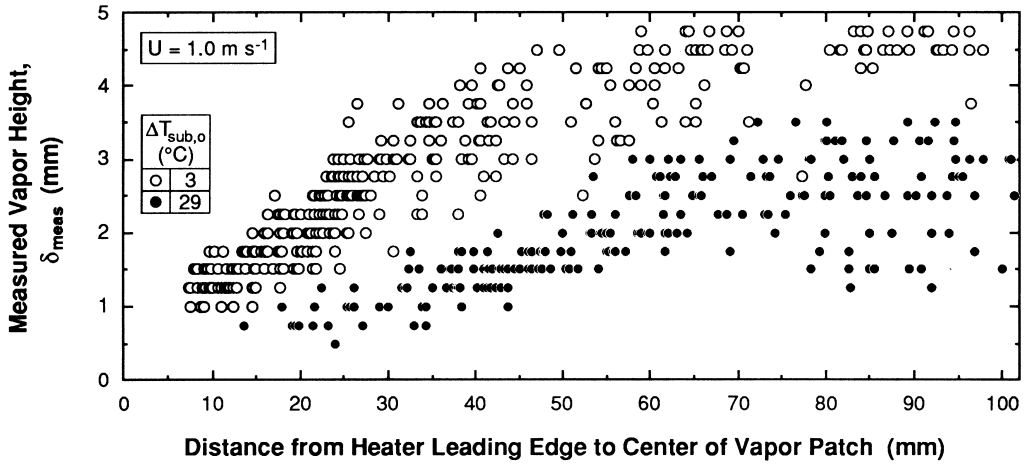

(a)

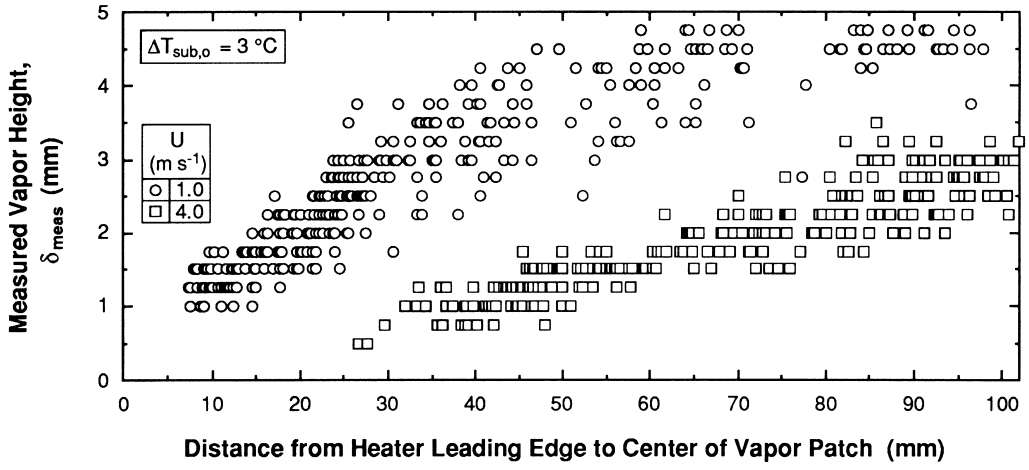

(b)

Fig. 11. Effect of (a) subcooling and (b) velocity on vapor development as indicated by the measured heights of all vapor patches observed at CHF.

and liquid length along the heated wall. For this case, the ratio of liquid-to-vapor length was $b \approx 0.3$. The increase in b over that for near-saturated conditions indicates subcooled flow is better at allowing liquid access to the heated surface.

4.4. Vapor shape analysis

In addition to obtaining measurements, the vapor patches were categorized based on shape to identify characteristics pertinent to CHF. By far the most common form observed was a generic, wave-like shape with no special features, as revealed by the video images in Fig. 7 and illustrated in Fig. 9(a). It was typically a vapor mass with maximum thickness near its center and tapered on the ends. This wave-like formation grew by the addition of newly-generated vapor and by coalescence with other vapor masses. It remained attached to the surface as it advected downstream, continuing to grow in size as it accumulated more vapor.

The overhanging vapor type, also illustrated in Fig. 9(a), was observed mostly for the highly subcooled case,

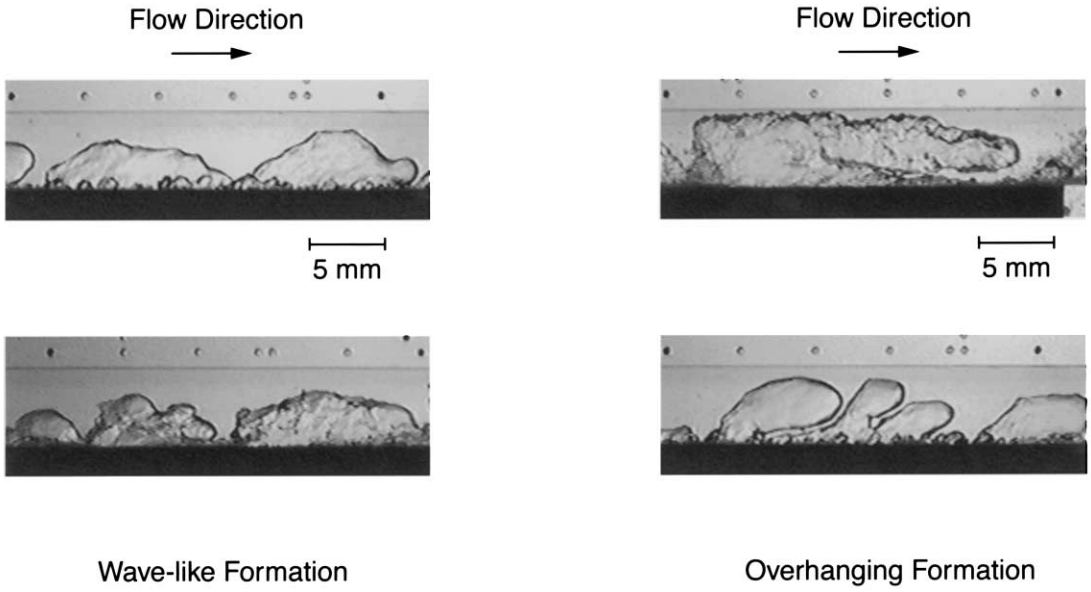

Fig. 12. Video images of wave-like and overhanging vapor formations.

though far less frequently than the wave-like type. This formation was created when the momentum of the newly created vapor was directed away from the wall toward the center of the channel where streamwise velocity is greater. The liquid momentum in the middle of the channel forced the vapor in the streamwise direction while the vapor remained in contact with the wall through surface tension forces, creating the overhanging formation. Once the trapped liquid was evaporated, rewetting of the surface by the cooler bulk was hindered by the interference of the overhanging vapor.

Figure 12 provides video images of the wave-like and overhanging formations observed in the flow channel. Statistical results reveal that the more frequently occurring shape was the wave-like formation. The overhanging vapor formation occurred typically less than 10% of the time. However, for subcooled flow ($\Delta T_{\mathrm{sub,o}} = 29^{\circ}\mathrm{C}$) at $U = 1$ m s^{-1}, it represented nearly one quarter of the observed patches over the downstream half of the heater.

5. Conclusions

Tests were conducted in a straight, rectangular channel subjected to one-sided heating providing critical heat flux data for broad ranges of velocity and subcooling. Vapor characteristics at CHF were analyzed by means of flow visualization techniques with the intention of incorporating the results into a CHF model. Key conclusions from this investigation are as follows:

(1) At critical heat flux, vapor coalesces into a series of patches that resemble a wavy, periodic vapor layer which propagates along the heated wall permitting liquid replenishment only at discrete locations (wetting fronts) between the vapor patches.
(2) Vapor patch length and height grow along the flow direction and decrease with increasing velocity and subcooling.
(3) The length of liquid–surface contact between vapor patches increases in the flow direction but remains proportional to the local vapor wavelength. The ratio of these two lengths is constant along the flow direction and for all velocities at the same subcooling.
(4) The liquid-to-vapor length ratio increases with increasing subcooling. In the present study, this ratio was 0.2 and 0.3 for near-saturated and highly subcooled conditions, respectively.
(5) The predominant vapor shape associated with CHF is the generic, wave-like formation. An overhanging vapor formation appears far less frequently, especially at near-saturated conditions.

Acknowledgements

The authors are grateful for the support of the Office of Basic Energy Sciences of the U.S. Department of Energy (Grant No. DE-FG02-93ER14394.A003). Financial support for the first author was provided through the Air Force Palace Knight Program.

References

[1] J.E. Galloway, I. Mudawar, CHF mechanism in flow boiling from a short heated wall—I. Examination of near-wall conditions with the aid of photomicrography and high-speed video imaging. International Journal of Heat and Mass Transfer 36 (1993) 2511–2526.

[2] J.E. Galloway, I. Mudawar, CHF mechanism in flow boiling from a short heated wall—II. Theoretical CHF model. International Journal of Heat and Mass Transfer 36 (1993) 2527–2540.

[3] C.O. Gersey, I. Mudawar, Effects of heater length and orientation on the trigger mechanism for near-saturated flow boiling critical heat flux—I. Photographic study and statistical characterization of the near-wall interfacial features. International Journal of Heat and Mass Transfer 38 (1993) 629–641.

[4] C.O. Gersey, I. Mudawar, Effects of heater length and orientation on the trigger mechanism for near-saturated flow boiling critical heat flux—II. CHF model. International Journal of Heat and Mass Transfer 38 (1995) 643–654.

[5] J.C. Sturgis, I. Mudawar, Critical heat flux in a long, rectangular channel subjected to one-sided heating—II: analysis of critical heat flux data. International Journal of Heat and Mass Transfer 42 (1999) 1845–1862.

[6] D.E. Maddox, I. Mudawar, Single- and two-phase convective heat transfer from smooth and enhanced microelectronic heat sources in a rectangular channel. ASME Journal of Heat Transfer 111 (1989) 1045–1052.

[7] P.S. Wu, T.W. Simon, Critical heat flux and subcooled flow boiling with small heated regions on straight and concave-curved walls. 10th International Heat Transfer Conference Vol. 7, Brighton, UK, (1994) 569–574.

[8] J.G. Collier, J.R. Thome, Convective Boiling and Condensation, 3rd edn. Clarendon Press, Oxford, 1994.